Exp.-Nr. **A2**
Eingang:
an PAC:

Mainz Microtron MAMI

A2 Collaboration at MAMI
Spokespersons: P. Pedroni, A. Thomas

Proposal for an Experiment

"Isospin asymmetry dependence of neutron skins with Coherent pion photoproduction"

Spokespersons for the Experiment :
D.P. Watts, University of Edinburgh, Edinburgh, UK
C. Sfienti, University of Mainz, Germany
L. Zana, University of Edinburgh, Edinburgh, UK

Abstract of Physics :
We propose to measure neutron skin properties for a range of nuclear targets using the recently established technique of coherent π^0 photoproduction. Target nuclei are chosen to cover a wide range of isospin asymmetry (I=N-Z/A), expanding significantly the range covered by the previous coherent π^0 measurements. The predicted linear scaling of the neutron skin size with isospin asymmetry will be used to extract tighter constraints on the asymmetry parameter of the equation of state for neutron matter. The new data will challenge state-of-the-art theoretical predictions of nuclear structure, based on nuclear density functional theories and and ab-initio techniques.

Abstract of Equipment :
The experiment will be performed at the tagged photon facility of MAMI (Glasgow Tagger) using Crystal Ball/TAPS detector setup together with particle identification detector (PID) and multi-wire proportional chambers (MWPCs).

MAMI Specifications :

beam energy	855 MeV
beam polarization	unpolarized

Photon Beam Specifications :

tagged energy range	140 – 800 MeV
photon beam polarization	Unpolarised

Equipment Specifications :

detectors	Crystal Ball/TAPS, PID, MWPCs
target	^{48}Ca, ^{56}Fe,^{112}Sn,^{204}Pb, ^{206}Pb

Beam Time Request :

set-up/test with beam	24 hours
data taking	636 hours

List of participating authors:

- **Institut für Physik, University of Basel, Switzerland**
  S. Abt, S. Garni, M. Günther, A. Käser, B. Krusche, S. Lutterer, M. Oberle, Th. Strub, N.K. Walford, L. Witthauer
- **Institut für Experimentalphysik, University of Bochum, Germany**
  G. Reicherz
- **Helmholtz–Institut für Strahlen- und Kernphysik, University of Bonn, Germany**
  F. Afzal, R. Beck, K. Spieker, A. Thiel
- **JINR, Dubna, Russia**
  N.S. Borisov, A. Lazarev, A. Neganov, Yu.A. Usov
- **SUPA School of Physics, University of Edinburgh, UK**
  M. Bashkanov, S. Kay, D.P. Watts, L. Zana
- **SUPA School of Physics and Astronomy, University of Glasgow, UK**
  J.R.M. Annand, D. Hamilton, D.I. Glazier, S. Gardner, K. Livingston, R.Macrae , I.J.D. MacGregor, C. Mullen, D. Werthmüller
- **Department of Astronomy and Physics, Saint Mary's University Halifax, Canada**
  A.J. Sarty
- **Racah Institute of Physics, Hebrew University of Jerusalem, Israel**
  G. Ron
- **Kent State University, Kent, USA**
  C.S. Akondi, D.M. Manley
- **Institut für Kernphysik, University of Mainz, Germany**
  P. Achenbach, H.J. Arends, M. Biroth, F. Cividini, A. Denig, P. Drexler, M.I. Ferretti-Bondy, W. Gradl, V.L Kashevarov, P.P. Martel, A. Neiser, E. Mornacchi, M. Ostrick, S.N. Prakhov, V. Sokhoyan, C. Sfienti, O. Steffen, M. Thiel, A. Thomas, S. Wagner, J. Wettig, M. Wolfes
- **University of Massachusetts, Amherst, USA**
  R.Miskimen, A. Rajabi
- **Institute for Nuclear Research, Moscow, Russia**
  G. Gurevic, R. Kondratiev, V. Lisin, A. Polonski
- **INFN Sezione di Pavia, Pavia, Italy**
  A. Braghieri, S. Costanza, P. Pedroni
- **Department of Physics, University of Regina, Canada**
  Z. Ahmed, G.M. Huber, D. Paudyal
- **Mount Allison University, Sackville, Canada**
  D. Hornidge
- **Tomsk Polytechnic University, Tomsk, Russia**
  A. Fix
- **George Washington University, Washington, USA**
  W.J. Briscoe, C. Collicott, E.J. Downie, I.I. Strakovski

- **Rudjer Boskovic Institute, Zagreb, Croatia**
  M. Korolija, I. Supek
- **Technische Universität Darmstadt, Darmstadt, Germany**
  T. Aumann

1 Introduction

Characterising the existence and nature of neutron skins in nuclei is one of the highest impact topics in modern nuclear physics, constraining not only nuclear theories but also the basic equation of state (EOS) for nucleonic matter. The neutron skin (Δr_{np}), defined as the difference in the root mean square radii between protons and neutrons, shows a strong correlation [3,15] with the most poorly established parameter in the EOS for neutron rich matter, the density dependence of the symmetry energy (L). The character of the neutron skin, therefore, has a wide impact and the potential to give important new information on neutron star structure and cooling mechanisms [6–10], searches for physics beyond the standard model [11,12], the nature of 3-body forces in nuclei [13, 14], collective nuclear excitations [15–18] and flows in heavy-ion collisions [19, 20].

We lead a major new programme with the CB@MAMI to determine neutron skins with electromagnetic (photon) probes for the first time, using coherent π^0 photoproduction. Our first measurement on ^{208}Pb [21] provided information on both the size and shape of the neutron skin and indicated the skin has a diffuse character. The broad impact of neutron skin measurements in nuclear physics, astrophysics and particle physics led to the article being selected as an editor's suggestion and for a public synopsis. The results have been used in numerous ongoing theoretical analyses to constrain L e.g. [22]. The analysis of the neutron skin for ^{40}Ca is being finalised, with preliminary results presented at recent conferences, including NuSym16, with publication anticipated in 2017. These results indicate a negative neutron skin for ^{40}Ca, the first time such a property has been measured, and in agreement with Energy Density Functional (EDF), cutting edge QCD based ab-initio nuclear theories [23] and recent quark-meson coupling functionals [24]. With the promising results for ^{40}Ca the stage is set for measurements on ^{48}Ca. The recent ab-initio calculations published in Nature [23] predict a smaller neutron skin for ^{48}Ca than predicted by any EDF based models. The authors highlight how the measurement on ^{48}Ca is therefore crucial to validate ab-initio methods and to potentially provide a normalisation for EDF approaches. Recent work has shown that the size of the neutron skin in ^{48}Ca can also put constraints on poorly understood 3-neutron forces, with an accuracy of 0.03 fm quoted to achieve this [arXiv:1606.03648, 2016].

The typical beamtime required to measure a neutron skin using the coherent π method is of the order of a few days. As well as the key ^{48}Ca measurement this offers the exciting possibility to measure neutron skins with accuracy over a wide range of isospin asymmetry, I=N-Z/A. Achieving this would provide tighter constraints on the extracted value of L (and on nuclear theory) as the skin is expected to scale linearly with I, with the gradient determined by L [15]. This method allows many data to be combined giving the possibility to achieve more accurate constraints than achievable for individual measurements. Our new proposed measurements ^{48}Ca, ^{56}Fe, ^{112}Sn, ^{204}Pb ,^{206}Pb and ^{238}U will provide data over a wide range of I enabling a leading and much needed constraints on the gradient.

The proposal will firstly outline the current status of the data analysis for the coherent pion photoproduction programme (section 2) and discuss competing methods (section 3). The proposed measurements and estimates of the uncertainties in the measured quantities are discussed in sections 4 and 5. The base equipment used in the A2 hall is discussed in section 6.

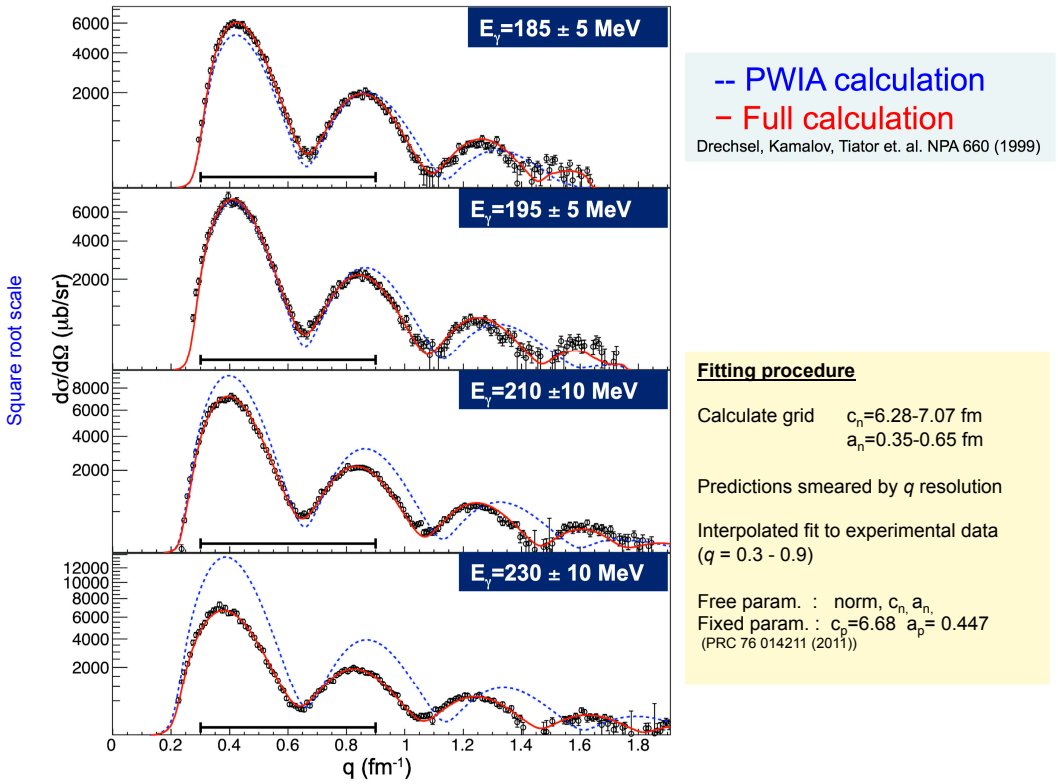

Figure 1: The measured differential cross section for coherent ^{208}Pb(γ, π^0), for four different E_γ bins. The fits to the data are shown by the red solid line. The blue line shows the same prediction in PWIA. Details of the fit parameters are shown in the figure.

2 Overview of current results on neutron skins from coherent pion photoproduction

2.1 ^{208}Pb results

Our result on ^{208}Pb [21] provided the first successful extraction of a neutron skin using an electromagnetic probe. The measured differential cross sections for the coherent ^{208}Pb(γ, π^0) reaction as a function of momentum transfer, q, are shown in Fig. 1. The coherent yield in each momentum transfer bin is extracted by a missing energy analysis in which the coherent yield and quasi-free pion production background are fitted for each bin. The details of this analysis are presented in the publication.

The differential cross section for ^{208}Pb(γ, π^0) is fitted with the theoretical model predictions, smeared by the experimental q resolution (red dashed line). The parameters of the 2-parameter Fermi distribution (2PF) for the charge distribution are fixed to the well determined experimental values from electron scattering and muonic atoms [32]. The parameters of the 2PF neutron distribution, half-height radius (c_n) and diffuseness

(a_n), are varied over a grid spanning the range c_n=6.28-7.07 fm and a_n=0.35-0.65 fm. A χ^2 minimising fit is used to extract the best fit parameters for the neutron distribution. For comparison also shown in the figure (blue dashed line) are the PWIA theoretical predictions for the best fit value of the neutron distribution, where the modelling of the π^0-nucleus interaction is removed. This allows the effect of the π^0-nucleus interaction in the model to be assessed. For the lower E_γ bins this is modest for the fitted region up to just above the 2nd maxima. This reflects the very small π-N interaction in this region, for which the mean free path is comparable even with the size of a large nucleus like ^{208}Pb. At higher E_γ the π-N interaction becomes much stronger, mainly as the larger π energies allow excitation of the Δ resonance. For these bins the maxima and minima are more significantly shifted by the π^0-nucleus in the final state. As the FSI effects vary in strength with E_γ the consistency of the extracted skin provides constraints on the modelling of this process as discussed in the paper.

The extracted parameters for the neutron distribution were Δr_{np}=0.15$\pm$0.03($stat.$)$^{+0.01}_{-0.03}$($sys.$) fm with half radius and diffuseness given by c_n=6.70$\pm$0.03($stat.$) fm and a_n=0.55$\pm$0.01($stat.$)$^{+0.02}_{-0.03}$($sys.$) fm respectively. The clean extraction of the coherent yield permitted both parameters of the 2PF neutron distribution to be constrained by the data. Changes in half radii produce shifts in the positions of the maxima and minima while the diffuseness mainly affects the relative heights of the 1st and 2nd maxima.

2.2 ^{40}Ca results

The clean extraction of the coherent yield for a medium mass nucleus, like ^{40}Ca is more complex than for a heavy nucleus like ^{208}Pb. The main reason is due to the relatively larger role of incoherent processes, comprising both quasi-free pion production and inelastic production where the final state nucleus is left in an excited state. These background processes broadly scale with A whereas the coherent processes scale with A^2 [37]. The analysis on ^{40}Ca is still in progress, but first extractions of the neutron skin have already been obtained, with publication expected in 2017. In this section the current status and future plans for the ^{40}Ca analysis will be presented.

For ^{40}Ca a significant inelastic contribution exists for higher momentum transfers. This can be seen in fig.2 where the fits to the missing energy distributions are shown for different q ranges. For momentum transfer near the first maxima, q=0.6 fm^{-1}, the coherent process dominates and little incoherent strength is evident. For q=0.8 fm^{-1} approaching the first minima the quasi-free background can be seen. However at higher q it is clear that additional strength is evident beyond the coherent and quasi-free π processes. For a first analysis additional gaussian contributions were added, offset from the centroid of the coherent strength by the excitation energies of the low lying excited states in ^{40}Ca. The properties of this inelastic contribution can also be assessed using a different method, exploiting the capability of the CB [42] to detect coincident nuclear gamma radiation from the excited nucleus. For ^{40}Ca the lowest excited state, the 3$^-$at 3.7 MeV, dominates with this γ energy clearly visible in the data [43]. As found in the missing energy fits there is negligible strength below q=0.7 fm^{-1}. This reflects the transition form factor for this state which falls off rapidly at low q. (note that for the ^{208}Pb analysis there was no evidence of any significant contribution of inelastic processes to the yield from nuclear decay gamma studies).

The extracted coherent yields are shown in Fig. 4. As a first step we have extracted the neutron skin only in the region of the first maxima (below q=0.7 fm^{-1}) where the inelastic yield is negligible. The two data sets in the figure show the cross sections with and without the fitting of the inelastic contribution. It can be seen that the experimental data from both extraction methods are almost identical for $q \leq$0.7 fm^{-1}. The model predictions are fitted to the data with the same procedure as for ^{208}Pb, with the diffuseness fixed to the average value of the theoretical predictions. The extracted skin is Δr_{np}=0.04$\pm$0.01($stat$). The description of the data at higher q outside the fitted region is satisfactory when the inelastic contribution is

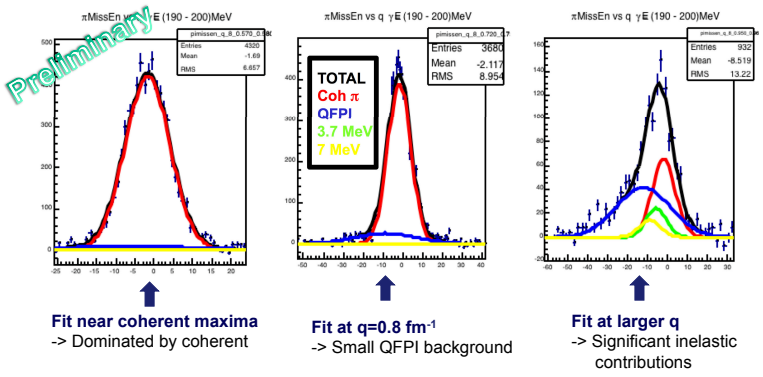

Figure 2: ^{40}Ca analysis. Typical missing energy fits for three different q bins. Experimental data points (black) are fitted with Coherent, quasi-free pion and inelastic contributions (see figure for key)

accounted for in the fit. Currently the method to remove the inelastic is being refined. The nuclear decay gamma information will allow much of its contribution to be removed prior to the fits. Optimising the fitting procedure and fit stability is currently being investigated using detailed simulation studies. With further work it looks promising that also the diffuseness can be extracted for ^{40}Ca.

2.3 ^{116}Sn, ^{120}Sn and ^{124}Sn results

We are finalising analysis of our data on an isotopic chain of tin [MAMI-A2-15-09]. The evolution of the neutron skin across an isotopic chain provides additional constraint on nuclear models and the extraction of L. Measurement of the increase of the skin across an isotopic chain also gives sensitivity to the nuclear models with an advantage that model dependent systematics in the absolute value of the skin can be reduced.

The current status of the data are shown in Fig.5. The change in the matter distribution can be clearly seen in the data for the different isotopes. A 0.1fm increase in skin would correspond to a shift of $\sim$1° in the angle of the diffraction minima, clearly evident in the data. The right panel shows the ratio of the cross sections for ^{124}S and ^{116}Sn versus pion angle. For identical matter form factors this ratio would be close to 1 for all angles. The structures in the data reflect the changes in the neutron skin. The line shows the model predictions assuming the properties predicted by a single EDF, FSUGold. The analysis in pion angle is close to completion. The next stage will be to move into the momentum transfer frame and apply the analyses used for ^{208}Pb and ^{40}Ca.

3 Neutron skin measurements with other methods

The potential impact of obtaining an accurate determination of Δr_{np} has led to a flurry of theoretical and experimental interest in recent years. Many studies have focused on ^{208}Pb which has a relatively well-

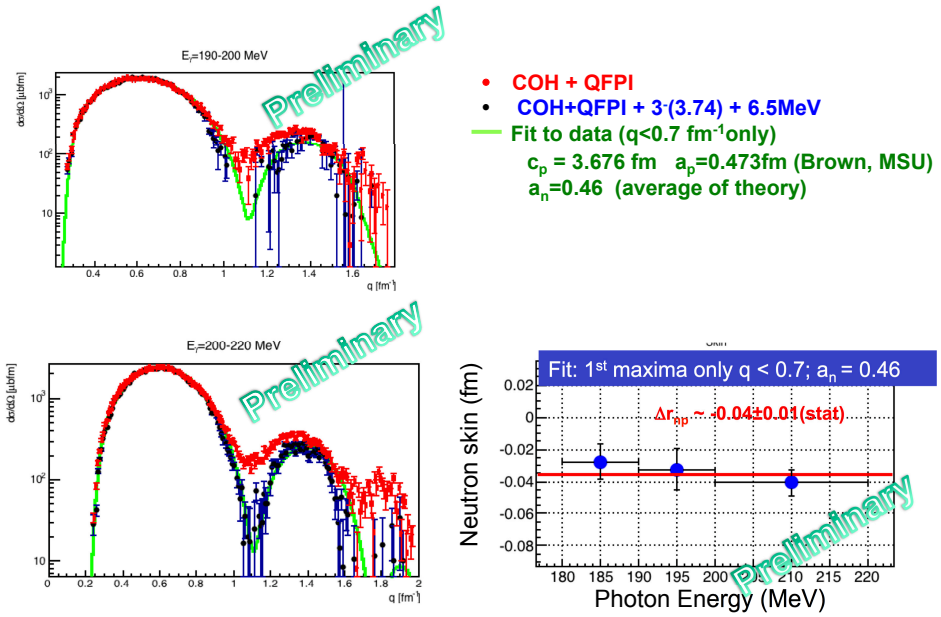

Figure 3: Preliminary analysis of the ^{40}Ca coherent π photoproduction data. The two panels on the left show the differential cross section plotted versus momentum transfer. The red data points show the results of fitting using the formula employed in the ^{208}Pb analysis, where the coherent yield and quasifree pion production background are fitted to the missing energy distributions in each q bin. The blue points show the results when inelastic strength is also fitted (see figure). The green line shows the fit of the theoretical model to the data, using only the region of q$\leq$0.7 fm^{-1} where the coherent process dominates (see text). Right panel shows the extracted neutron skin for three different E_γ bins.

understood structure due to the closed proton (Z=82) and neutron (N=126) shells. A goal of a $\pm$0.05 fm accuracy in Δr_{np} is quoted [2] as the requirement to constrain the equation of state sufficiently to remove the current major ambiguities. A recent review of the experimental attempts to measure Δr_{np} in ^{208}Pb is given by Tsang *et. al.* [13]. Recent analysis of proton [25] and pion [30] scattering data gave Δr_{np}=0.211$\pm$0.06 fm and Δr_{np}=0.16$\pm$0.07 fm respectively. Studies of the annihilation of antiprotons on the nuclear surface [28, 29] gave Δr_{np}=0.18$\pm$0.04($expt.$) $\pm$ 0.05($theor.$) fm. Isospin diffusion in heavy-ion collisions gave Δr_{np}=0.22$\pm$0.04 fm [31]. Measurements of pygmy dipole resonances and electric dipole polarizabilities of nuclei [16, 18, 33] gave Δr_{np} ranging from 0.156 fm to 0.194 fm with quoted accuracies as small as $\pm$0.024 fm, although the model dependence is still debated [34] and an accuracy of $\pm$0.05 fm is taken in Ref. [13]. A measurement using an electroweak probe has been obtained in parity-violating electron scattering on nuclei (PREX-1), utilising the preferential coupling of the exchanged weak boson to neutrons. A first measurement at a single momentum transfer gave Δr_{np}=0.33$\pm$0.17 fm in ^{208}Pb [38].There are proposals to make further measurements of neutron skins in parity violating e- scattering (PREX-II). A recent readiness review at JLAB showed the issues in PREX-I could be overcome, where electronics and vacuum

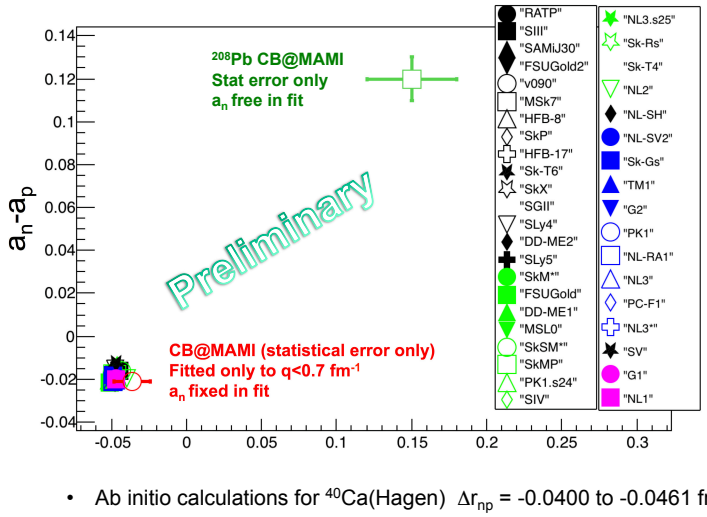

- Ab initio calculations for ^{40}Ca(Hagen) Δr_{np} = -0.0400 to -0.0461 fm

Figure 4: ^{40}Ca analysis. Data points show the ^{40}Ca and ^{208}Pb results plotted as diffuseness (y-axis) versus neutron skin (x-axis), The EDF predictions for ^{40}Ca are shown by the symbols (key in figure))

failures arising from to unexpectedly high beam-related radiation dose compromised the statistical accuracy. PREX-II on ^{208}Pb is expected to run in 2017. There is also a CREX proposal to measure the neutron skin on ^{48}Ca using the target made available from Oak Ridge. There are further plans for measurements with the parity-violating technique at the new MESA facility in Mainz.

The only other measurement where a wide range of isospin was sampled are the studies of the annihilation of antiprotons on the nuclear surface [28,29]. The interpretation and accuracy of these data are debated, with uncertainties arising from the sensitivity of the measurement only to the far tails of the nucleon distributions (average interaction distance of 9 fm compared to an rms radius of 5.45fm), with the resulting requirement for large extrapolations to the nuclear interior. The root-mean-square neutron radius is not directly measured, making the skin thickness results strongly dependent on theoretical models. The systematic uncertainty is taken as $\pm$0.05fm in global analyses [13]. The statistical accuracy of the available data is typically poorer than other methods as can be seen in Fig. 6 . For ^{40}Ca the error in the skin determination from antiprotonic measurements was $\sim$0.09 fm.

Other attempts to determine the neutron skin in ^{48}Ca are in progress. Proton scattering measurements at close to zero degrees give information on the dipole polarisability which enables a model dependent determination of the skin. The latest progress can be seen Ref. [44].

4 Count rate estimates and beam time request

The count rate estimates have been obtained by scaling from the data on ^{40}Ca and ^{208}Pb to achieve similar statistical accuracy with the new measurements. The scaling takes account of the achievable densities for the proposed targets and the attainable beam flux. The statistics to be obtained will permit a statistical accuracy of 0.03 fm in the neutron skin when using a simultaneous fit to the half radii and diffuseness of the

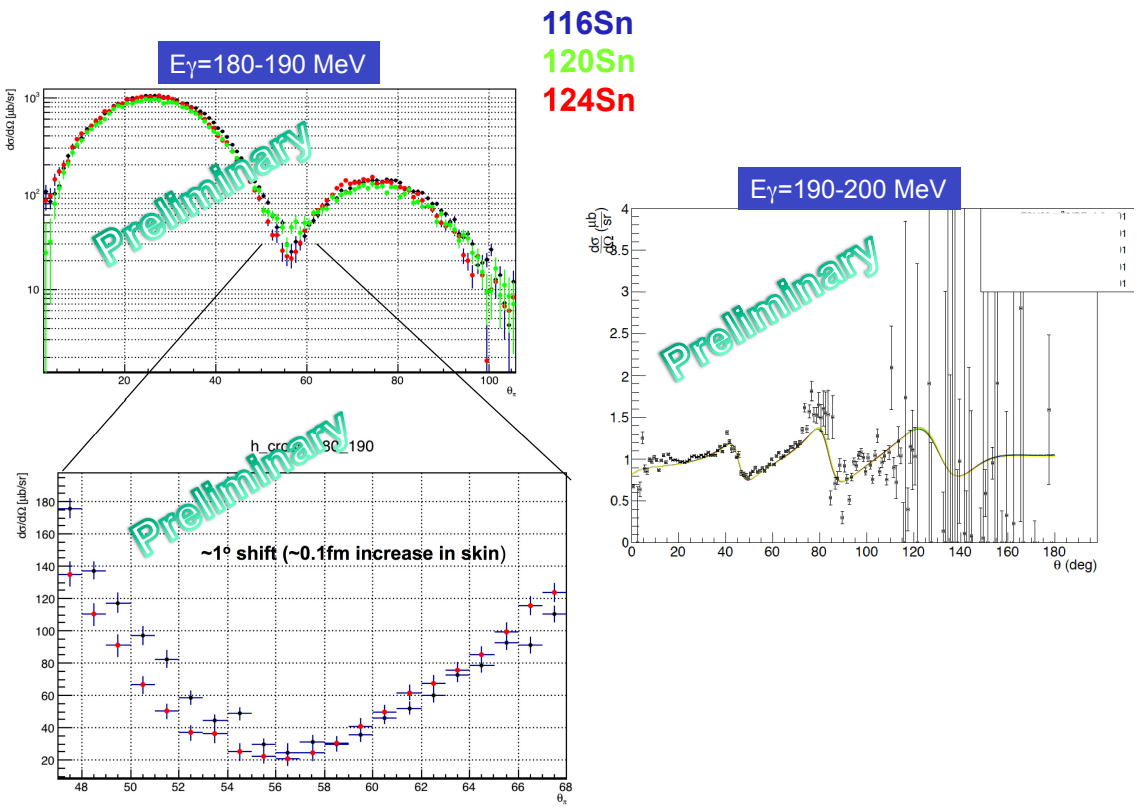

Figure 5: Tin analysis: Left plots show the differential cross section plotted versus pion angle (degrees). The coloured symbols correspond to the different targets (see key in figure). The lower plot shows an enlarged plot of the minima region. Right plot shows the ratio of the differential cross section for ^{124}Sn to ^{116}Sn.

neutron distribution, as seen for the ^{208}Pb analysis. However, it should be noted that this is an upper limit. As discussed for the ^{40}Ca analysis when the diffuseness is already constrained by theory then a 1 parameter fit to extract the skin using only the first maxima/minima allows statistical error of ∼0.01-0.02.

Table 1 gives estimates of the required beamtimes for each target. The estimates assume the same run conditions as the previous datataking with a collimator of 3mm, multiplicity 2 trigger in the CB and electron beam energy of 855 MeV. The maximum achievable photon flux is now a factor of 5 larger than available during these earlier run periods giving the opportunity to use thinner targets, a distinct advantage when isotopically pure target material is required. Where thin targets will be used we have assumed running at the maximum flux of the new tagger (maximum of 5×10^6 per tagger channel). Where thicker targets are available we use the tagger flux used in the previous beamtime (maximum of 1×10^6 per tagger channel) so as to run with comparable DAQ livetimes. The scaling of the cross section for the coherent production process by A^2 is also accounted for when extrapolating from the existing data. The beamtime for a proposed targets, t_{target}, is calculated from

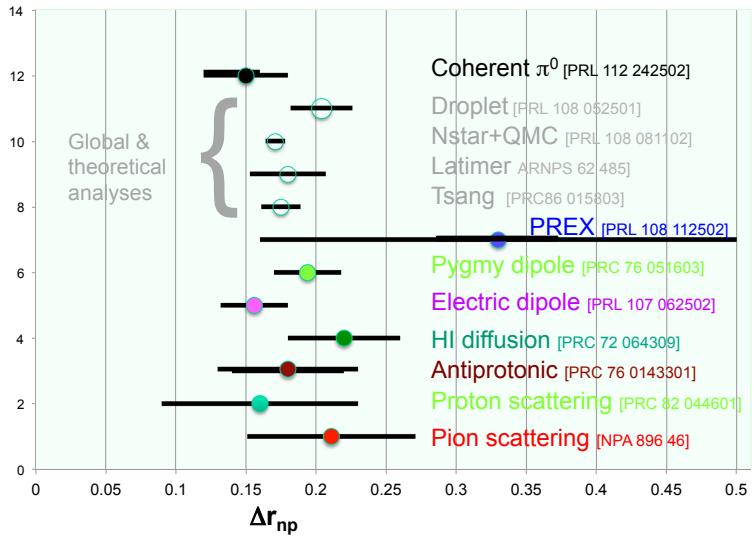

Figure 6: Summary of previous measurements of the neutron skin thickness in ^{208}Pb. The unfilled data points are from global or theoretical analyses. The filled data points are from measurements. Where statistical and systematic errors are both stated the systematic error is shown by the upper error bar on each data point.

$$t_{target} = \frac{\rho_{target}}{\rho_{ref}} \times \frac{\gamma flux^{target}}{\gamma flux^{ref}} \times \frac{A^2_{target}}{A^2_{ref}} \times t_{ref}$$

where the subscripts $target$ and ref refer to the proposed and reference (^{208}Pb or ^{40}Ca) targets respectively.

The isotopic lead targets (used in previous A1 experiments) are taken as thickness ∼115 mg cm^{-2} [45]. The ^{48}Ca target material will use existing material available from GSI [46] providing 17 mg cm^{-2}. The additional material to get to 50 mg cm^{-2} will be sourced from UK and German funding agencies if the proposal is approved. The ^{112}Sn properties are based on an existing target at GSI. The expected accuracy of the proposed data is illustrated in Fig. 7, where data points showing the expected accuracy of the measurement are plotted versus I (note that except for ^{40}Ca and ^{208}Pb the points are placed arbitrarily in the y axis - see caption). The statistical accuracy in the neutron skin determination is assumed to be similar to that obtained for the ^{208}Pb analysis, as comparable π^0 yields will be obtained. The error for ^{40}Ca is smaller as the diffuseness is strongly restricted by theory, so that a single parameter fit for the neutron skin can be employed using information only from the 1st maxima. This method may also be possible for other nuclei with small isospin asymmetry and theoretical analyses of the range of diffuseness predicted by EDF theories are currently underway by the Barcelona group. The gray band in Fig.7 shows the current constraint on the slope from ref. [15]. It is clear that the CB@MAMI coherent pion data has the potential

Table 1: Table showing the proposed targets and expected statistical accuracies in the neutron skin when using a 2 parameter fit (with diffuseness as a free parameter) or a one parameter fit where the diffuseness is fixed from theory.

Target	ρ (mg/cm^2)	γ flux	Time (days)	A^2_{target}/A^2_{ref}	$\delta\Delta r_{np}$ (stat) 2 par	$\delta\Delta r_{np}$ (stat) 1 par
^{208}Pb	836	1×10^6	2	-	0.03	0.02
^{40}Ca	1550	1×10^6	2	-	0.03	0.01
^{48}Ca	50	5×10^6	10	1.4 rel. to ^{40}Ca	0.03	0.02
^{56}Fe	115	5×10^6	3	1.9 rel. to ^{40}Ca	0.03	0.02
^{112}Sn	1443	1×10^6	2	7.8 rel. to ^{40}Ca	0.03	0.02
^{204}Pb	115	5×10^6	3	0.9 rel. to ^{208}Pb	0.03	0.02
^{206}Pb	115	5×10^6	3	1.0 rel. to ^{208}Pb	0.03	0.02
^{238}U	115	5×10^6	2.5	1.3 rel. to ^{208}Pb	0.03	0.02
Empty	-	5×10^6	3	-	-	-
Total			26.5			

to provide a new independent determination of the slope, using a completely different experimental method with different (and smaller) systematic uncertainties.

4.1 Systematic errors

A first estimate of the systematic errors associated with the coherent pion photoproduction method to extract neutron skins was obtained for the previous ^{208}Pb analysis. The main sources are discussed below:

- **1) Photon flux:** The skin properties are extracted from the shape of the differential cross section. In the extraction of the skin an overall normalisation is included in the fit which will negate errors in the absolute flux determination. For the previous ^{208}Pb analysis this normalisation was within $\pm5\%$. This variation is consistent with the experimental systematic in the determination of the photon flux.

- **2) Pion detection efficiency:** Overall offsets in the magnitude of the detection efficiency are accounted for by the normalisation in the fit. The analysis uses the CB alone to use a symmetric and well understood detector system. Any theta (or equivalently q) dependent effects were investigated by comparing the skins extracted using all q or at different q regions (first,second,third minima). No statistically significant q dependent effects were observed.

- **3) Pion angle reconstruction:** The target position influences the reconstructed pion angle and therefore the evaluation of q. The target position is extracted using information from 2-track charged particle events in the MWPC and it's position in z could be evaluated to within 0.5mm. From evaluation of simulated data a shift of the target by 1cm gives a 1° offset in π^0 angle, corresponding to $\sim$0.1fm systematic in Δr_{np}. Therefore for 0.5mm the systematic error in Δr_{np} is estimated to be of order 0.005 fm. The reconstruction of the π^0 angle in the CB was assessed using simulated data where the actual pion angle for each event could be compared to the reconstructed pion angle - using the same software and analysis as used for the real data. The average difference between these 2 quantities was consistent with zero with point to point variation less than 0.01 degrees.

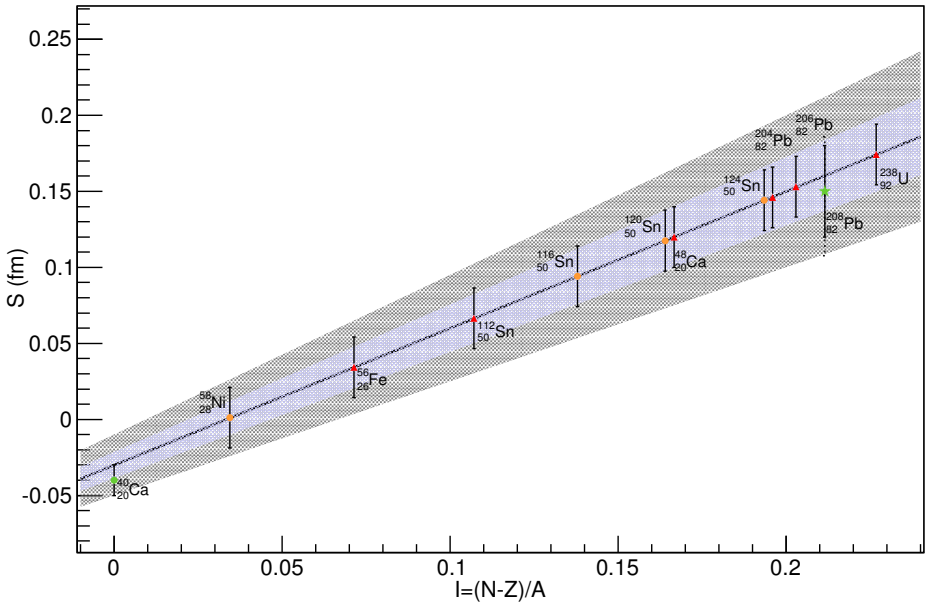

Figure 7: Overview of the coherent pion measurement programme, showing the expected statistical accuracy of the neutron skin determination for the different measurements, plotted versus I. The statistical errors are those expected from a one parameter fit (with diffusness taken from theory). The neutron skins extracted for ^{208}Pb and the preliminary ^{40}Ca result are shown by the green symbols. The other data points show *only* the expected statistical accuracy in the neutron skin from a 1 parameter fit to the experimental data, with the symbols placed arbitarily in the y axis on the average line from ref [15]. Orange symbols show coherent pion data which has already been obtained and is currently under analysis. The red symbols show the expected accuracy of the measurements proposed here. The dark grey band shows the constraint on the slope obtained in Ref. [15]. The light blue band shows the expected statistical error in the determination of the slope using just the coherent pion data. The estimated systematic errors are discussed in the text.

- **4) Target density:** The surface density of the experimental targets can be measured to less than 2%. The error should not affect the extracted value due to the inclusion of an overall normalisation in the fit

- **5) Tagging efficiency:** The tagging efficiency (probability that an electron hit in the tagger focal plane results in a photon at the target) is obtained in runs where a ∼100% efficiency lead glass photon detector is placed in the beam. For a 3mm collimator efficiencies of 44-48% are expected for the E_γ range where the skin is extracted. The data is analysed in small E_γ bins of width ± 5 MeV. Variations in tagging efficiency over the bin are small and residual systematics in the magnitude of the photon flux will be taken into account in the normalisation.

- **Model dependence in neutron skin extraction:** The extraction of the skin relies on the theoretical model. Model dependencies were assessed in the ^{208}Pb analysis and are summarised below. The same procedures will be applied to all the targets measured in the programme allowing a deeper and broader investigation of potential systematics. The measurement of neutron skins over a wide range, -0.04

to 0.16fm and over a wide range of mass numbers will give the extensive dataset to challenge the theoretical model. The model used to extract the neutron skins was developed by Drechsel, Tiator and Kamalov [55]. It is currently being further developed by Vanderhaeghen at MITP. The main improvements will be (i) the ability to input exact form factor shapes, rather than a 2PF distribution (ii) exploration of different treatments of pion-nucleus FSI and iii) inclusion and study of systematics in using different PWA for the pion production amplitude.

6) Photon energy dependence of the skin extraction: For the ^{208}Pb analysis the half radii showed no statistically significant variation with E_γ. The extracted diffuseness showed consistency except for the highest E_γ bin, where the FSI effects are very large, and a 3σ variation in the extracted diffuseness was observed. This was included in the quoted systematic errors in the paper. No statistically significant variation of the neutron skin parameters was observed when fitting in different θ_π (or q) ranges out to the third maxima. For these latter studies the diffuseness was fixed to the range of values predicted by theory and the reduction of the number of fit parameters allowed a statistical error of below $\pm$0.02fm in the extracted skin.

7) Modelling of the π-nucleus interaction: From Fig. 1 it can be seen that the model gives a good description of the data for all q - even outside of the range used in the fit. At high q there is a large lever arm and the FSI effects have a more significant effect in shifting the minima. Despite this the model still describes the position of the 3rd maxima to an accuracy better than $\sim$10%. Assuming the same error in the shifts produced in the region around the 1st minima allows a rough estimate of systematics from modelling of the π-A interaction. This gives an estimated systematic of less than 0.01 fm in the low q region where the skin is extracted.

8) Modelling of the π-production amplitudes: The model uses pion photoproduction amplitudes from the MAID PWA. Variation of the magnitude of the proton and neutron coupling by $\pm$5%, the level of agreement between the MAID and SAID PWA predictions, resulted in an estimated systematic of 0.02 in the diffuseness. This systematic may be reduced following further developments of the theoretical model which will allow different PWA parameterisations of the amplitude to be compared.

9) Modelling of the nucleon distributions: The model uses a 2PF approximation for the nucleon distributions. There has been recent theoretical work showing that this is a good approximation for ^{208}Pb and ^{40}Ca [47], and that next order improvements such as 3PF parameterisations would not significantly change the result. However, the capability to include 3PF or actual nucleon distributions will be available in future versions of the model.

10) Agreement of radial distributions with well known nuclei: A further assessment of model dependent systematics was obtained by studying the isospin symmetric nucleus, ^{40}Ca, for which all theories agree on the size of the (negative) neutron skin. The agreement between our data and the theoretical predictions within the statistical errors gives further constraint on potential model dependent systematics for the method.

- **Summary of estimated systematic errors:** For a 2-parameter fit to the data (diffuseness and neutron skin) we expect systematics comparable with the published work on ^{208}Pb for each of the nuclei, corresponding to $\sim \pm$0.02fm in diffuseness and $\sim \pm$0.03fm in the neutron skin. As discussed in the paper the systematics will have some dependence on the measured consistency of the extracted skin, diffuseness over different E_γ bins and any q dependencies. It is not possible to know beforehand what agreement will be observed and if the new data will reveal additional model dependencies. The overall systematic error in the diffuseness (and skin) may be reduced with the expected improvements in the production amplitude, which should reduce systematic error (8) above.

When using a 1-parameter fit (diffuseness fixed from nuclear theory) and using the method of just fitting the momentum transfer distributions at low q (as described for the analysis of the ^{40}Ca data), then a systematic error in the extracted skin arises from the variation of the diffuseness in the nuclear model predictions. For a typical isospin asymmetric nucleus (^{48}Ca and ^{208}Pb) the variation in the diffuseness from the full range of different density functionals (excluding outliers NL2 and SV1 as done in Ref. [23]) is around 0.05fm which corresponds to a systematic of ∼0.015fm in the neutron skin. Therefore the combined systematic for the skin from this method (including (3) and (7) above) would be expected to be $\sim \pm 0.02$fm. Again, this error assumes that no statistically significant E_γ or q dependent effects are observed in the analysis for the different targets.

5 Summary

The proposed measurements of coherent π^0 photoproduction will provide new and valuable data regarding the size and nature of neutron skins in nuclei. This will include a key measurement of ^{48}Ca, which has recently become amenable to ab-initio calculation. The programme will also measure the neutron skin across the full range of isospin symmetry observed for stable nuclei, where it is predicted to range from a negative neutron skin up to ∼0.16fm. The measured dependence of the neutron skin on isospin symmetry will provide further new constraints on our understanding of neutron skins in nuclei and the equation of state for nuclear matter.

6 Experimental apparatus

6.1 Photon Beam

The A2 photon beam is derived from the production of Bremsstrahlung photons during the passage of the MAMI electron beam through a thin radiator. The resulting photons can be circularly polarised, with the application of a polarised electron beam, or linearly polarised, in the case of a crystalline radiator. The degree of polarisation achieved is dependent on the energy of the incident photon beam (E_0) and the energy range of interest, but currently peaks at ∼75 % for linear polarisation (Fig. 8) and ∼85 % for circular polarisation (Fig. 9). The maximum degree of linear polarisation should be further improved by 5 to 10 % by the end of 2009 when the collimation and beam monitoring systems will be optimised for MAMI-C during the installation of the Frozen Spin Target. The Glasgow-Mainz Photon Tagger (Fig 10) provides energy tagging of the photons by detecting the post-radiating electrons and can determine the photon energy with a resolution of 2 to 4 MeV depending on the incident beam energy, with a single-counter time resolution $\sigma_t = 0.17$ ns [62]. Each counter can operate reliably to a rate of ~ 1 MHz, giving a photon flux of 2.5×10^5 photons per MeV. Photons can be tagged in the momentum range from 4.7 to 93.0% of E_0.

To augment the standard focal plane detector system and make use of the Tagger's intrinsic energy resolution of 0.4 MeV (FWHM), there exists a scintillating fibre detector ("Tagger Microscope") that can improve the energy resolution by a factor of ∼6 for a ∼100MeV wide region of the focal plane (dependent on its position) [63].

6.2 Frozen-spin target

Polarization experiments using high density solid-state targets in combination with tagged photon beams can reach the highest luminosities. For the double polarisation measurements planned with the Crystal Ball detector on polarized protons and deuterons a specially designed, large horizontal ^{3}He/^{4}He dilution

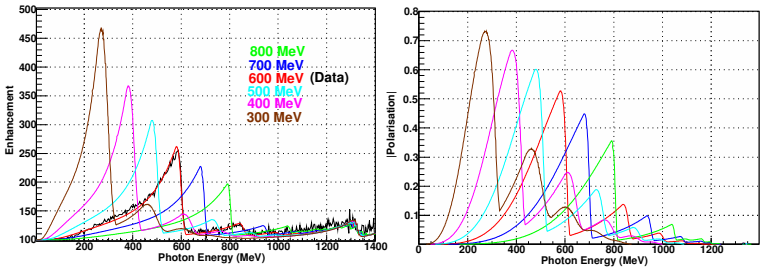

Figure 8: Linear polarisation available with the current collimation system for a variety of crystal orientations. The thin black lines are data obtained during recent MAMI-C runs.

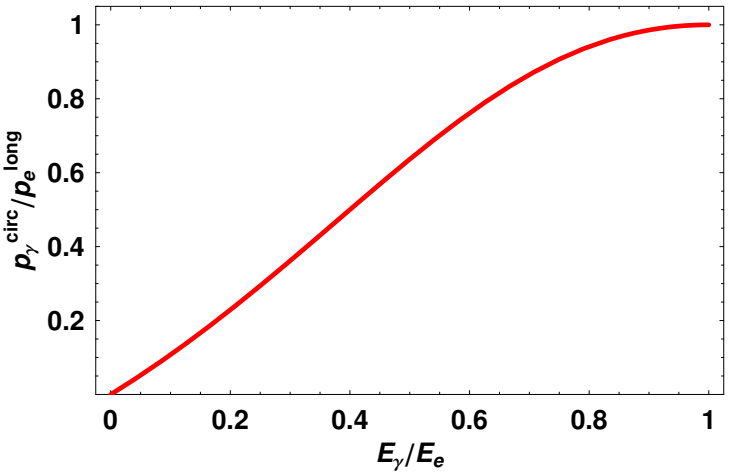

Figure 9: Helicity transfer from the electron to the photon beam as function of the energy transfer. The MAMI beam polarisation is P_e =85%.

refrigerator was built in cooperation with the Joint Institute for Nuclear Research (JINR) Dubna (see Figure 11). It has minimum limitations for the particle detection and fits into the central core of the inner Particle Identification Detector (PID 2). This was achieved by using the frozen spin technique with the new concept of placing a thin superconducting holding coil inside the polarization refrigerator. Longitudinal and transverse polarisations are possible.

Highest nucleon polarization in solid-state target materials is obtained by a microwave pumping process, known as dynamic nuclear polarization (DNP). This process is applicable to any nucleus with spin and has already been used in different experiments with polarized proton and deuteron targets. The geometric configuration of the target is the same for the polarized proton and neutron setup. However, since the polarization measurement of the deuteron is more delicate due to the small size of the polarization signals, the modification of some basic components is needed. The reason for this is twofold: firstly the magnetic moment of the deuteron is smaller than that of the proton and, in addition, the interaction of the deuteron quadrupole moment with the electric field gradient in the sample broadens the deuteron polarization signal. An accuracy $\delta P_p/P_p$ of 2 - 3% for the protons and $\delta P_D/P_D$ of 4 - 5% for the deuterons is expected in the polarization measurement. It has also to be taken into account that the measured deuteron polarization P_D is not equal to the neutron polarization P_n. Assuming a 6 % admixture of the D-state of the deuteron, a calculation based on the Clebsch-Gordon coefficients leads to $P_n = 0.91\ P_D$. Several polarized proton and

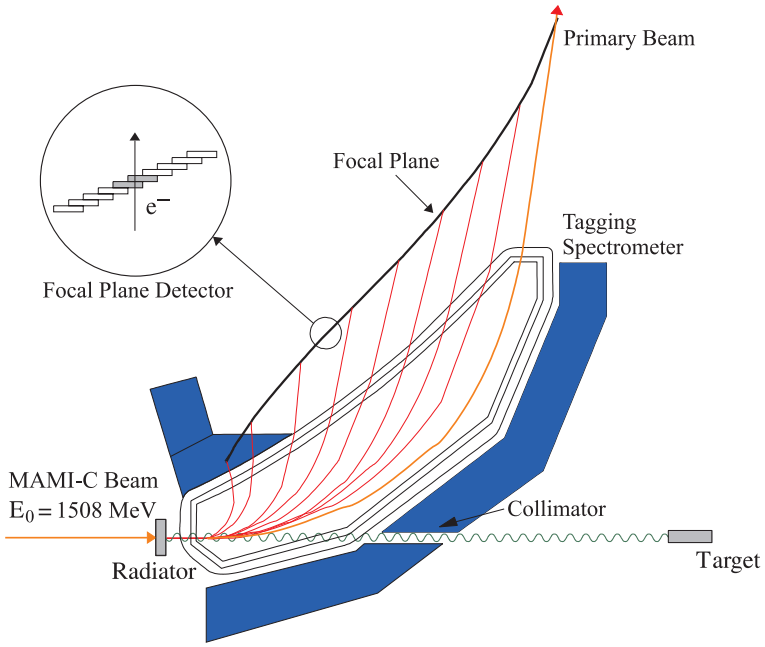

Figure 10: The Glasgow-Edinburgh-Mainz photon tagging spectrometer

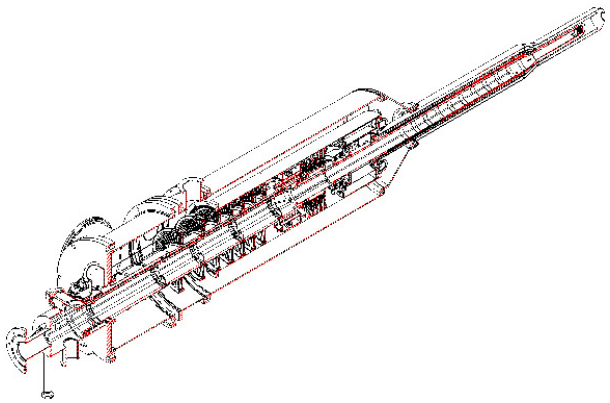

Figure 11: The new dilution refrigerator for the Crystal Ball detector

deuteron materials are available such as alcohols and deuterated alcohols (e.g. butanol $C_4H_{10}O$), NH_3, ND_3 or ^{6}LiD. The most important criteria in the choice of material suitable for particle physics experiments are the degree of polarization P and the ratio K of free polarizable nucleons to the total number of nucleons. Further requirements on polarized target materials are a short polarization build-up time and a simple, reproducible target preparation. The polarization resistance against radiation damage is not an issue for experiments with a low intensity tagged photon beam ($I_\gamma \approx 5 \times 10^7 \gamma$ /sec) as will be used here. However, the limitations of a reduced relaxation time due to overheating of the target beads (Kapitza resistance) will have to be investigated.

Taking all properties together, butanol and deuterated butanol are the best material for this experiment. For protons we expect a maximum polarisation of $P_p = 90$ % and an average polarisation of $P_p = 70$ % in the frozen spin mode. Recently, a deuteron polarization $P_D = 80$ % was obtained with Trityl doped butanol targets at 2.5 T magnetic field in a ^{3}He/^{4}He dilution refrigerator. At a 0.4 T holding field an average neutron polarization P_n (see above) of 50 % will be obtained. The filling factor for the $\approx$ 2mm diameter butanol spheres into the 2cm long, 2cm diameter target container will be around 60 %. The experience from the GDH runs in 1998 [64] shows that, with a total tagged photon flux of 5×10^7, relaxation times of about 200h can be expected. The polarization has to be refreshed by microwave pumping every two days.

In conclusion, we estimate that we will achieve the following target parameters:

- Maximum total tagged photon flux in the energy range of 4 - 95% E_0: $I_\gamma \approx 5 \times 10^7 \gamma sec^{-1}$, with relaxation time of 200 hours.
- Target proton density in 2cm cell: $n_T \approx 9.1 \times 10^{22} cm^{-2}$(including dilution and filling factors)
- Average proton polarisation $P_p = 70$ %
- Target deuteron density in 2cm cell: $n_T \approx 9.4 \times 10^{22} cm^{-2}$(including dilution and filling factors)
- Average neutron polarisation $P_n = 50$ %

6.3 Crystal Ball Detector System

The central detector system consists of the Crystal Ball calorimeter combined with a barrel of scintillation counters for particle identification and two coaxial multiwire proportional counters for charged particle tracking. This central system provides position, energy and timing information for both charged and neutral particles in the region between 21° and 159° in the polar angle, θ, and over almost the full azimuthal (ϕ) range. At forward angles, less than 21°, reaction products are detected in the TAPS forward wall. The full, almost hermetic, detector system is shown schematically in Fig. 12 and the measured two-photon invariant mass spectrum is shown in Fig. 13.

The Crystal Ball detector is a highly segmented 672-element NaI(Tl), self triggering photon spectrometer constructed at SLAC in the 1970's. Each element is a truncated triangular pyramid 41 cm (l5.7 radiation lengths) long. The Ball has an energy resolution of $\Delta E/E = 0.020(E[GeV])^{0.36}$, an angular resolution in σ_θ of $2 - 3°$ and σ_ϕ of $\sigma_\theta / \sin\theta$ for electromagnetic showers [65]. The readout electronics for the Crystal Ball were completely renewed in 2003, and it now is fully equipped with SADCs which allow for the full sampling of pulse-shape element by element. In normal operation, the onboard summing capacity of these ADCs is used to enable dynamic pedestal subtraction and the provision of pedestal, signal and tail values for each element event-by-event. Each CB element is also newly equipped with multi-hit CATCH TDCs. The readout of the CB is effected in such a way as to allow for flexible triggering algorithms. There is an analogue sum of all ADCs, allowing for a total energy trigger, and also an OR of groups of sixteen crystals

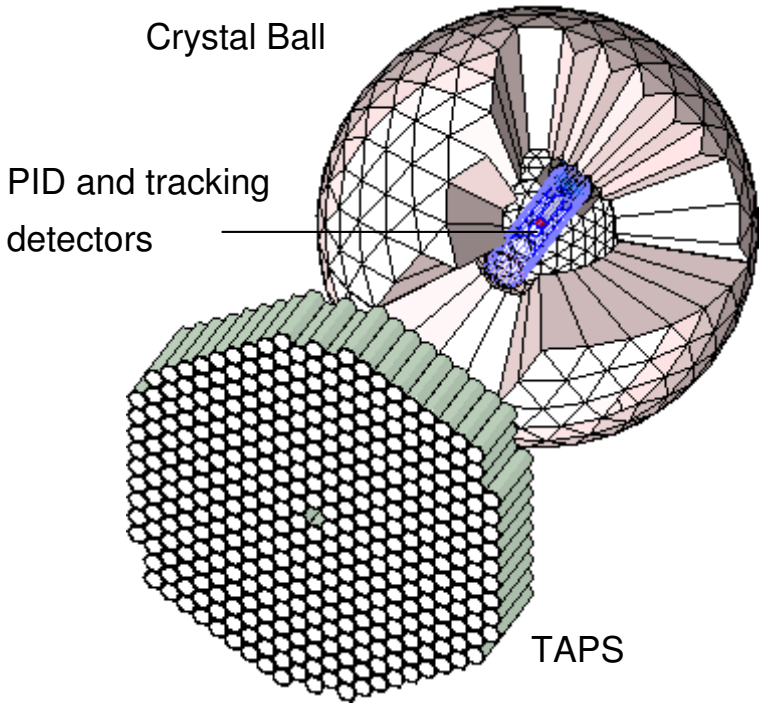

Figure 12: The A2 detector setup: the Crystal Ball calorimeter with cut-away section showing the inner detectors and the TAPS forward wall.

to allow for a hit-multiplicity second-level trigger - ideal for use when searching for high multiplicity final states.

In order to distinguish between neutral and charged particles species detected by the Crystal Ball, the system is equipped with PID 2, a barrel detector of twenty-four 50 mm long 4 mm thick scintillators, arranged so that each PID 2 scintillator subtends an angle of 15° in ϕ. By matching a hit in the PID 2 with a corresponding hit in the CB, it is possible to use the locus of the ΔE, E combination to identify the particle species (Fig. 14). This is primarily used for the separation of charged pions, electrons and protons. The PID 2 covers from 15° to 159° in θ.

The excellent CB position resolution for photons stems from the fact that a given photon triggers several crystals and the energy-weighted mean of their positions locates the photon position to better than the crystal pitch. For charged particles which deposit their energy over only one or two crystals, this is not so precise. Here the tracks of charged particles emitted within the angular and momentum acceptance of the CB detector will be reconstructed from the coordinates of point of intersections of the tracks with two coaxial cylindrical multiwire proportional chambers (MWPCs) with cathode strip readout. These MWPCs are similar to those installed inside the CB during the first round of MAMI-B runs [66]. The most significant difference is that all detector signals are taken at the upstream end of the MWPCs, minimising the material required and facilitating particle detection in the forward polar region.

A mixture of argon (79.5%), ethane (30%) and freon-CF_4 (0.5%) is used as the filling gas. This mixture is a compromise between charge multiplication and localization requirements imposed by the ionizing particle tracks.

Within each chamber both the azimuthal and the longitudinal coordinates of the avalanche will be evaluated form the centroid of the charge distribution induced on the cathode strips. The location of the hit

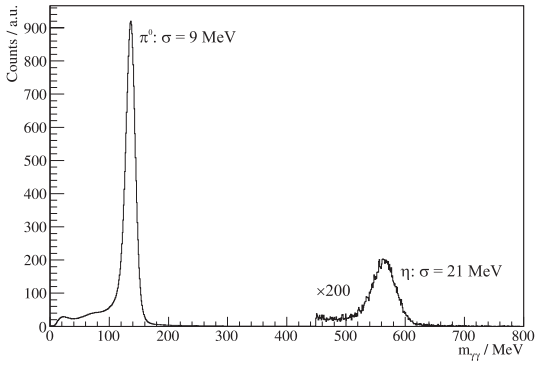

Figure 13: Two gamma invariant mass spectrum for the CB TAPS detector setup. Both η and π^0 mesons can be clearly seen.

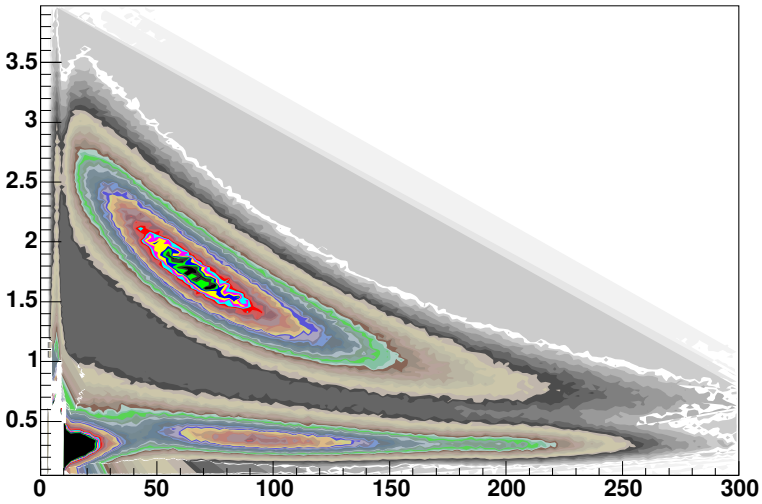

Figure 14: A typical ΔE/E plot from the PID detector. The upper curved region is the proton locus, the lower region contains the pions and the peak towards the origin contains mostly electrons.

wires(s) will be used to resolve ambiguities which arise from the fact that each pair of inner and outer strip cross each other twice. The expected angular resolution (rms) will be $\approx 2^\circ$ in the polar emission angle ϑ and $\approx 3^\circ$ in the azimuthal emission angle φ.

The MWPCs have been recently installed inside the CB frame and their calibration using both cosmic rays and test beam data is currently underway.

6.4 TAPS Forward Wall

The TAPS forward wall is composed of 384 BaF_2 elements, each 25cm in length (12 radiation lengths) and hexagonal in cross section, with a diameter of 59 mm. Every TAPS element is covered by a 5 mm thick plastic veto scintillator. The single counter time resolution is $\sigma_t = 0.2$ ns. The energy resolution can be described by the $\Delta E/E = 0.018 + 0.008/(E[GeV])^{0.5}$ [65]. The angular resolution in the polar angle is better than 1°, and in the azimuthal angle it improves with increasing θ, being always better than 1/R radian, where R is the distance in centimeters from the central point of the TAPS wall surface to the point on the surface where the particle trajectory meets the detector. The TAPS readout was custom built for the beginning of the CB@MAMI program and is effected in such a way as to allow particle identification by Pulse-Shape Analysis (PSA), Time-of-Fight (TOF) and ΔE/E methods (using the energy deposit in the plastic scintillator to give ΔE). TAPS can also contribute to the CB multiplicity trigger and is currrently divided into up to six sectors for this purpose.

References

[1] M. Gmitro, S.S. Kamalov and R. Mach, Phys. Rev. C36 1105 (1987).

[2] R.J. Furnstahl, Nucl. Phys. A706 85 (2002).

[3] Phys. Rev. C 81, 051303(R) (2010).

[4] B. G. Todd-Rutel and J. Piekarewicz Phys. Rev. Lett. 95, 122501 (2005).

[5] B.A. Brown, Phys. Rev. Lett. 85, 5296 (2000); S. Typel and B.A. Brown, Phys. Rev. C 64, 027302 (2001).

[6] A.W. Steiner, M. Prakash, J.M. Lattimer, and P.J. Ellis, Phys. Rep. 411, 325 (2005).

[7] C.J. Horowitz and J. Piekarewicz, Phys. Rev. Lett. 86, 5647 (2001).

[8] J. Xu *et. al.*, Astrophys. J. 697, 1549 (2009).

[9] A.W. Steiner, J.M. Lattimer, and E.F. Brown, Astrophys. J. 722, 33 (2010).

[10] B.G. Todd-Rutel and J. Piekarewicz, Phys. Rev. Lett. 95, 122501 (2005).

[11] De-Hua Wen, Bao-An Li, and Lie-Wen Chen, Phys. Rev. Lett. 103, 211102 (2009).

[12] S.J.Pollock and M.C. Welliver, Phys. Lett. B464 177 (1999)

[13] M.B. Tsang *et. al.*, Phys. Rev. C 86, 015803 (2012).

[14] K. Hebeler, J. M. Lattimer, C. J. Pethick and A. Schwenk, Phys.Rev. Lett. 105, 161102 (2010)

[15] M. Centelles, X. Roca-Maza, X. Viñas, and M. Warda, Phys. Rev. Lett. 102, 122502 (2009).

[16] A. Carbone *et. al.*, Phys. Rev. C 81, 041301(R) (2010).

[17] L.W. Chen *et. al.*, Phys. Rev. C 82, 024321 (2010).

[18] A. Tamii *et. al.*, Phys. Rev. Lett. 107, 062502 (2011).

[19] B.A. Li, L.W. Chen, and C.M. Ko, Phys. Rep. 464, 113 (2008).

[20] M.B. Tsang *et. al.*, Phys. Rev. Lett. 102, 122701 (2009).

[21] C.M. Tarbert, D.P. Watts, D.I. Glazier *et. al.*, Phys. Rev. Lett. 112, 224502 (2014).

[22] C. Xu *et. al.*, Phys. Rev. C 90, 064310 (2014).

[23] G. Hagen *et. al.*, Nature Physics 12, 186 190 (2016).

[24] J.R. Stone *et. al.*, Phys. Rev. Lett. 116 092501 (2016).

[25] J. Zenihiro, H. Sakaguchi, T. Murakami, M. Yosoi, Y. Yasuda, S. Terashima, Y. Iwao, H. Takeda, M. Itoh, H. P. Yoshida, and M. Uchida, Phys. Rev. C 82, 044611 (2010)

[26] J. Jastrzebski *et. al.*, Int. J. Mod. Phys. E 13, 343 (2004).

[27] J. Piekarewicz, Nucl. Phys. A778 10 (2006).

[28] B. Klos *et. al.*, Phys. Rev. C 76, 014311 (2007).

[29] B. A. Brown, G. Shen, G. C. Hillhouse, J. Meng, and A. Trzcinska, Phys. Rev. C 76, 034305 (2007).

[30] E. Friedman, Nucl. Phys. A 896 46 (2012).

[31] L. W. Chen, C. M. Ko, and B. A. Li, Phys. Rev. C 72, 064309

[32] J. Arrington *et. al.*, Phys. Rev. C 76 014211 (2011)

[33] A. Krasznahorkay *et. al.*, Phys. Rev. Lett. 66, 1287 (1991); arxiv:1311.1456 (2013).

[34] P.G Reinhard and W. Nazarewicz, Phys. Rev. C 81, 051303(R) (2010).

[35] R.A. Schrack *et. al.*, Phys. Rev. **127** 1772 (1962).

[36] Y. Maghrbi *et. al.*, Eur. Phys. J. A49 (2013) 38

[37] B. Krusche, Eur. Phys. J. A**26** 7 (2005).

[38] S. Abrahamyan *et. al.*, Phys. Rev. Lett. 108, 112502 (2012).

[39] A. Starostin *et. al.*, Phys. Rev. C 64, 055205 (2001).

[40] I. Anthony, J.D. Kellie, S. J. Hall, G. J. Miller and J. Ahrens, Nucl. Instr. Meth. A301, 230 (1991) and S.J. Hall, G.J. Miller, R. Beck and P. Jennewein, Nucl. Instr. Meth. A368 698 (1996).

[41] K.-H. Kaiser *et. al.*, Nucl. Instr. Meth. A 593, 159 (2008).

[42] C.M. Tarbert *et. al.*, Phys. Rev. Lett 100, 132301 (2008).

[43] More details on this analysis can be found in the presentation of Watts at Nskins16 "https://indico.mitp.uni-mainz.de/event/47/timetable/20160518"

[44] e.g. see talk of Von Neumann Cosel at Nskins16 "https://indico.mitp.uni-mainz.de/event/47/timetable/20160518"

[45] Nucl. Phys. A 298, Issue 3, 1978, 452

[46] T. Aumann, Private communication.

[47] Phys. Rev. C 90, 067304 (2014).

[48] D. Watts, in Proc. of the 11th Int. Conf. on Calorimetry in Part. Phys., Perugia, Italy 2004, (World Scientific, Singapore, 2005, p. 560).

[49] G. Audit *et. al.*, Nucl. Instr. Methods A, 301 (1991), p. 473.

[50] S. Agostinelli *et. al.*, Nucl. Instr. Meth. A 506, 250 (2003).

[51] V.L. Kashevarov *et. al.*, Phys. Rev. C85, 064610 (2012).

[52] W. J. Briscoe, I. I. Strakovsky, and R. L. Workman, Institute of Nuclear Studies of The George Washington University Database;
http://gwdac.phys.gwu.edu/analysis/pr_analysis.html.

[53] The MAID analyses are available through the Mainz website: `http://wwwkph.kph.uni-mainz.de/MAID/`. See also D. Drechsel, S. S. Kamalov, and L. Tiator, Eur. Phys. J. A **34**, 69 (2007).

[54] The Bonn-Gatchina analyses are available through the Bonn website: `http://pwa.hiskp.uni-bonn.de/`. See also A. V. Anisovich, *et. al.*, Eur. Phys. J A **48**, 15 (2012).

[55] D. Drechsel *et. al.*, Nucl. Phys. A645 145 (1999).

[56] B. Krusche *et. al.*, Phys. Lett. B526 (2002) 287

[57] To check the validity of approximating $\rho(r)$ by a single 2pF distribution, the Fourier transforms of $\rho(r)$ and the fitted 2pF distribution were compared. In the momentum range up to q=0.9 fm^{-1}, over which the (γ,π^0) cross section was fitted to extract information about $\rho_n(r)$, the fractional difference between the two transforms only rises to 0.3% at q=0.9 fm^{-1}.

[58] M. Warda, X. Viñas, X. Roca-Maza, and M. Centelles, Phys. Rev. C 81, 054309 (2010).

[59] M. Centelles, X. Roca-Maza, X. Viñas, and M. Warda, Phys. Rev. C 82, 054314 (2010); X. Roca-Maza, M. Centelles, X. Viñas, and M. Warda, Phys. Rev. Lett. 106, 252501 (2011)

[60] M. Warda, X. Viñas, X. Roca-Maza and M. Centelles, Phys. Rev. C 80, 024316 (2009).

[61] Geometrical Relationships of Macroscopic Nuclear Physics' by R.W. Hasse and W.D. Myers, Springer Verlag, Heidelburg, 1988.

[62] J. C. McGeorge et al. Upgrade of the Glasgow photon tagging spectrometer for Mainz MAMI-C. *Eur. Phys. J. A*, 2008.

[63] A. Reiter et al. A microscope for the Glasgow photon tagging spectrometer in Mainz. *Eur. Phys. J. A*, 2006.

[64] A. Thomas et al. The GDH experiment at MAMI. *Nucl. Phys. B*, 79:591, 1999.

[65] S. Prakhov et al. Measuremrent of the slope parameter α for the $\eta \to 3\pi^0$ decay with the Crystal Ball dectector at the Mainz Microtron (MAMI-C). *Phys. Rev. C*, 79(035204), 2009.

[66] G. Audit et al. DAPHNE: a large-acceptance tracking detector for the study of photoreactions at intermediate energies. *Nucl. Instr. Meth. A*, 301:473, 1991.